The Aromatic Enhancement in the Axial-Flow Spherical Packed-Bed Membrane Naphtha Reformers in the Presence of Catalyst Deactivation

Mohammad Reza Rahimpour, Davood Iranshahi, Ehsan Pourazadi, Khadijeh Paymooni, and Ali Mohammad Bahmanpour
Dept. of Chemical Engineering, School of Chemical and Petroleum Engineering, Shiraz University, Shiraz 71345, Iran

DOI 10.1002/aic.12529
Published online February 28, 2011 in Wiley Online Library (wileyonlinelibrary.com).

Because of some disadvantages of conventional tubular reactors (CTRs), the concept of spherical membrane reactors is proposed as an alternative. In this study, it is suggested to apply hydrogen perm-selective membrane in the axial-flow spherical packed-bed naphtha reformers. The axial flow spherical packed-bed membrane reactor (AF-SPBMR) consists of two concentric spheres. The inner sphere is supposed to be a composite wall coated by a thin Pd-Ag membrane layer. Set of coupled partial differential equations are developed for the AF-SPBMR model considering the catalyst deactivation, which are solved by using orthogonal collocation method. Differential evolution optimization technique identifies some decision variables which can manipulate the input parameters to obtain the desired results. In addition to lower pressure drop, the enhancement of aromatics yield by the membrane layer in AF-SPBMR adds additional superiority to the spherical reactor performance in comparison with CTR. © 2011 American Institute of Chemical Engineers *AIChE J,* 57: 3182–3198, 2011

Keywords: catalytic naphtha reforming, spherical membrane reactor, orthogonal collocation method, DE optimization technique

Introduction

The main idea of the catalytic naphtha reforming process is to achieve a rich aromatic product stream, which is suitable as a gasoline blend stock. The feed is a hydro treated naphtha stream. The naphtha feed constitutes typically 15–30% by weight of the crude oil and is separated from the middle section of the atmospheric distillation tower.[1] Hydrogen is another important substance in the modern refineries, which is produced during the catalytic reforming process. Hydrogen has become increasingly valuable because it is used in hydro processing units for sulfur and nitrogen removal as well as the hydro cracking process.[1,2] Because there is an increasing demand for reformate, a minimal revamp of the process improvement is required to maximize refiners existing asset utilization.[1] Because of the importance and impact of the naphtha reforming unit on the overall refinery profits, it would be useful to revamp the reforming strategies to gain more benefits.[1,3] Therefore, many researchers have focused on this subject. First, a group of researchers tried to find a proper reaction network such as: Smith[4] (as a pioneer), Weifeng et al.,[5] Stijepovic et al.,[6] Ramage et al.,[7,8]

Correspondence concerning this article should be addressed to M. R. Rahimpour at rahimpor@shirazu.ac.ir.

Krane et al.,[9] Kmak,[10] Marin et al.,[11] and Juarez and Macias.[12] Furthermore, Li et al.,[13] Mostafazadeh and Rahimpour,[14] Weifeng et al.,[15] Rahimpour,[16] Taskar and Riggs,[17] Juarez et al.,[18] and Iranshahi et al.[19] have enhanced the production of more valuable products by means of optimizing and improving operating conditions. The last attempts were on the catalyst preparation and the effect of coke deposition on the catalyst surface. The studies in this field were carried out by Pieck et al.,[20] Martin et al.,[21] Ren et al.,[22] Borgna et al.,[23] Viswanadham et al.,[24] and Carvalho et al.[25]

The increasing demand for hydrogen has led to a revival in methods of hydrogen separation from gas mixtures in petroleum refineries and petrochemical industries in recent years.[26,27] As hydrogen separation occurs at high temperature and pressure, membranes are acceptable choices for hydrogen separation in the refineries. A Pd–Ag membrane layer with the silver content of 23–25% is extensively used for hydrogen separation.[28,29] As many as 100 membrane plants have been installed in refineries; the opportunity exists in other refineries to use this technology for hydrogen production.[30] Key requirements for the successful development of palladium-based membranes are low cost and high selectivity when accompanied by considerable mechanical/thermal and long term stability.[31] Unemotoa et al.[32] measured the hydrogen permeation rate through a Pd–Ag 23 wt % alloy membrane at temperatures up to 873 K.

The aim objective of this study is to investigate the performance and the capability of using axial flow spherical packed-bed membrane reactor (AF-SPBMR) in comparison with conventional tubular reactor (CTR). The superiority of AF-SPBMR configuration in comparison with CTR and tubular packed-bed membrane reactor (TMR) is briefly outlined as follows:

- Significantly lower pressure drop in comparison with CTR and TMR and consequently lower required power supply of recompression.
- Lower pressure drop permits the possibility of using smaller catalyst particles, which eliminates the internal mass transfer limitation.
- The possibility of using higher feed flow rate and increasing the plant productivity.
- Lower fabrication costs due to a reduction in the reactor thickness.[33]
- A great reduction in the membrane surface area in use and the related costs. The membrane surface area in use reduces 37.18%, 33.73%, and 29.10% for each reactor compared with TMR.

The feed maldistribution and the possibility of two-dimensional flow regimes are probably the most drawbacks of AF-SPBMR configuration. Using specific devices such as flow distributors along the reactor may be necessary. Furthermore, more studies are needed on the possibility of fabricating spherical membrane and also special attention should be paid to the membrane and its maintenance.

The effect of applying Pd–Ag membrane layer in the axial-flow spherical packed-bed reactors on products yield is investigated in this study. Most of the parameters of the system such as heat capacity, viscosity, molecular weight, density, and total molar flow rate are taken into consideration as variable parameters. Because spherical reactors (Sphs) have much lower pressure drop compared with CTR, they can operate at higher feed flow rates. In other words, the inlet flow rate to Sphs can be increased multifold (i.e., flow augmentation) in comparison with CTR. However, a flow ratio augmentation has a negative effect on products yield. As will be illustrated, differential evolution (DE) optimization technique is applied to compensate this undesired effect. The results show that the performance of AF-SPBMR improves significantly in comparison with CTR.

Table 1. Rate Constants and Heat of Reactions for Naphtha Reforming

$k = A \exp(B - E/1.8T)$	A	B	E (kJ/kmol)	ΔH (kJ/kmol of H_2)
k_{f_1}	9.87	23.21	36,350	71038.06
k_{f_2}	9.87	35.98	58,550	−36953.33
k_{f_3}	1	42.97	63,800	−51939.31
k_{f_4}	1	42.97	63,800	−56597.54
k_{e_1}	1.04×10^{-3}	46.15	46,045	–
k_{e_2}	9.87	−7.12	8000	–

Kinetics of Reactions

To investigate the kinetics of multicomponent naphtha mixture, a kinetic scheme is considered based on Smith's model.[4] The four related reactions are as follows:

$$\text{Naphthenes } (C_nH_{2n}) \leftrightarrow \text{Aromatics } (C_nH_{2n-6}) + 3H_2 \quad (1)$$

$$\text{Naphthenes } (C_nH_{2n}) + H_2 \leftrightarrow \text{Paraffins } (C_nH_{2n+2}) \quad (2)$$

$$\text{Naphthenes } (C_nH_{2n}) + n/3H_2 \leftrightarrow \text{Lighter ends } (C_1\text{—}C_5) \quad (3)$$

$$\text{Paraffins } (C_nH_{2n+2}) + (n-3)/3H_2 \leftrightarrow \text{Lighter ends } (C_1\text{—}C_5) \quad (4)$$

The corresponding reaction rates are as follows:

$$r_1 = \left(\frac{k_{f_1}}{K_{e_1}}\right)(k_{e_1}p_n - p_a{p_h}^3) \quad (5)$$

$$r_2 = \left(\frac{k_{f_2}}{K_{e_2}}\right)(k_{e_2}p_n p_h - p_p) \quad (6)$$

$$r_3 = \left(\frac{k_{f_3}}{p_t}\right)p_n \quad (7)$$

$$r_4 = \left(\frac{k_{f_4}}{p_t}\right)p_p \quad (8)$$

The reaction rate constants (k_{f_i}), equilibrium constants (K_{e_i}), activation energies (E_i), and standard heat of reactions ($\Delta H_{2898\ K}$) are presented in Table 1.[34]

More details about the reactions and how to find the activation energy can be found in previous publication.[14]

Process Description

Conventional tubular reactor

Some of the desirable reactions which take place in catalytic naphtha reforming process are highly endothermic. The catalytic naphtha reforming process has higher efficiency at

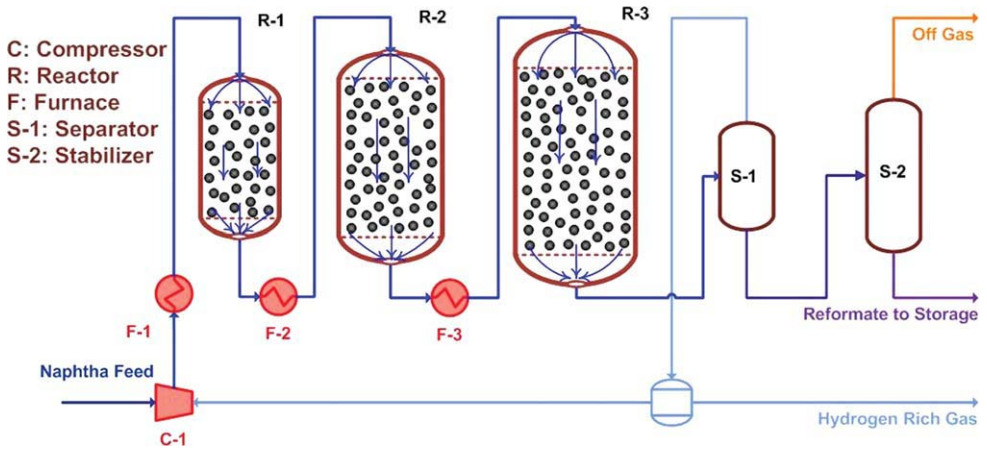

Figure 1. A simple process flow diagram for catalytic naphtha reforming process.

[Color figure can be viewed in the online issue, which is available at wileyonlinelibrary.com.]

high temperatures. Figure 1 shows a simplified scheme for the traditional naphtha reforming process in tubular reactors (tub). Liquid naphtha feed is mixed with a recycled gas stream containing 60–90% hydrogen. The recycled hydrogen can adjust the H_2/HC molar ratio through the reactors to prevent polymerization and coke formation, which can increase the risk of catalyst deactivation. The total reactor charge is preheated and directed to the first reactor. It flows axially through the packed-bed reactor and chemical reactions take place on the surface of the catalyst. The reactor discharge stream should be preheated in interstage kilns before entering the next reactor. The effluent from the last reactor is cooled, and then enters the separators which produce reformates as the bottom products. Table 2 shows the specific properties and operating conditions of the conventional process.

Conceptual scheme for an axial-flow spherical packed-bed membrane reactor

Because of some disadvantages of CTR such as high pressure drop along the reactor, high manufacturing costs, and low production capacity, the alternative choice of using Sphs is proposed. A novel idea in Sphs is the application of a membrane layer for hydrogen removal from the reaction side to shift the thermodynamic equilibrium to the products side. Membrane technology can be easily assisted in AF-SPBR, whereas it is hard to be applied in radial flow spherical packed-bed reactor. A schematic diagram of AF-SPBMR for naphtha reforming process is presented in Figure 2a. As it is shown in Figure 2b, AF-SPBMR consists of two concentric spheres in which the surface of the inner sphere is coated by a hydrogen perm-selective membrane layer. According to Uemiya,[35] self-supporting metallic membranes specially Pd based ones become unattractive for hydrogen separation in most cases due to their high cost, low permeance, and low chemical stability. Consequently, these membranes are generally prepared as thin films on porous support to provide a mechanical support. Catalysts are situated in the inner sphere (tube side). The naphtha feed flows axially through the packed-bed of the inner sphere. The sweeping gas which has a similar composition analysis to the recycled stream (0.695 mol % hydrogen) enters the outer sphere (shell side). Hydrogen is produced as a result of chemical reactions on the surface of the catalyst. Hydrogen permeates through the Pd–Ag membrane layer to the shell side and the sweeping gas carries the permeated hydrogen. According to the Le Chatelier's Principle, the reaction is shifted toward the product side mainly due to hydrogen removal from the reaction side. Thus, higher product yields are achieved in AF-SPBMR in comparison with CTR. The cross-sectional area is smaller in the inlet and the outlet of the inner sphere and it causes a significant pressure drop. Therefore, it is preferred to fill the space between the two perforated screens with catalysts. These perforated screens act as a mechanical support and cause more uniform feed

Table 2. Specifications of Reactors, Feed, Product, and Catalyst of Plant for Fresh Catalyst

Parameter	Numerical Value	Unit
Naphtha feed stock	30.41×10^3	kg/h
Reformate	24.66×10^3	kg/h
H_2/HC mole ratio	4.74	–
LHSV	1.25	h^{-1}
Mole percent of hydrogen in recycle	69.5	–
Diameter and length of first reactor	1.25, 6.29	m
Diameter and length of second reactor	1.67, 7.13	m
Diameter and length of third reactor	1.98, 7.89	m
Distillation fraction of naphtha feed and reformate		
TBP	Naphtha feed (°C)	Reformate (°C)
IBP	106	44
10%	113	73
30%	119	105
50%	125	123
70%	133	136
90%	144	153
FBP	173	181
Typical properties of catalyst		
d_p	1.2	mm
Pt	0.3	wt %
Re	0.3	wt %
S_a	220	m^2/g
ρ_B	0.3	kg/l
ε	0.36	–

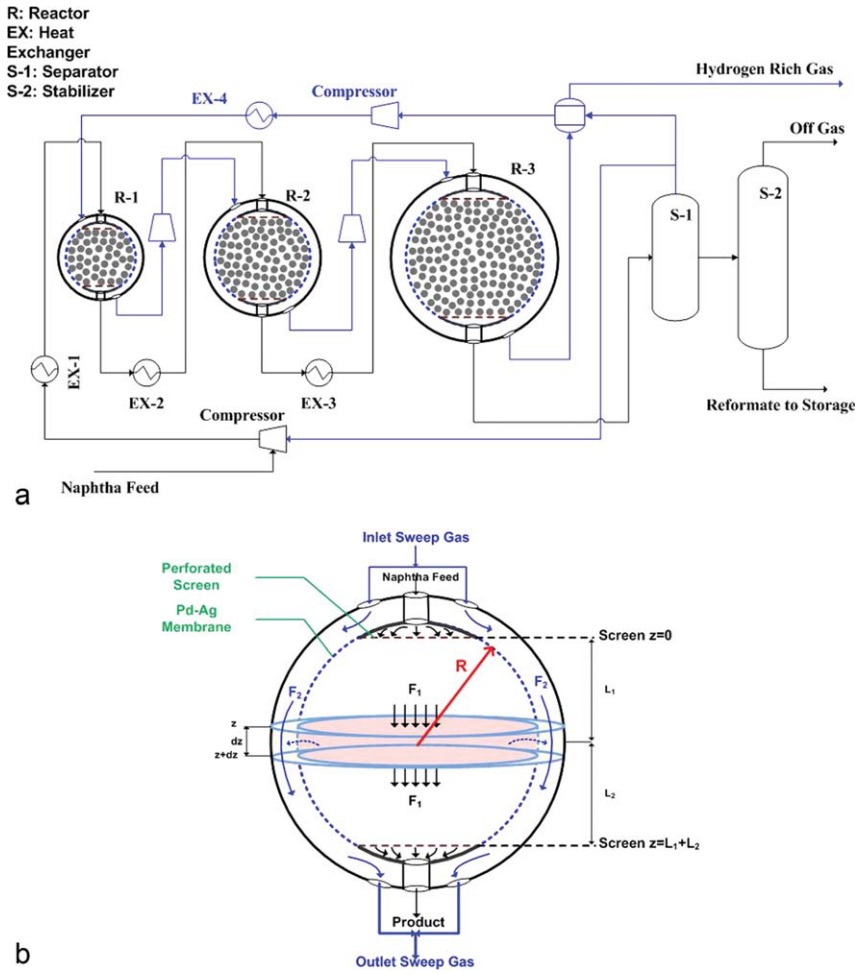

Figure 2. Schematics for (a) process flow diagram and (b) flow pattern of spherical membrane reactor in catalytic naphtha reforming.

[Color figure can be viewed in the online issue, which is available at wileyonlinelibrary.com.]

distribution. The specific properties and operating conditions of spherical configuration are reported in Table 3.

Mathematical Modeling

AF-SPBMR model

As shown in Figure 3, a computation element with the thickness of dz is taken into consideration. The parts related to the inner and the outer spheres are clearly recognized in this element. The situation of the membrane can be seen in this figure. The naphtha feed with a flow rate of F_1 enters, reacts, and eventually leaves the element of the inner sphere, whereas the hydrogen permeates through the membrane layer. The sweeping gas with a flow rate of F_2 enters, carries the permeated hydrogen and leaves the element of the outer sphere. The mass and energy balance equations obtained by analyzing this element are written for both sides. They must be coupled with the deactivation model,[36] pressure drop model[37] and also thermodynamic and kinetic relations as well as auxiliary correlations for predicting the AF-SPBMR performance. In this study, a homogeneous one-dimensional (1-D) model has been taken into consideration. The results of the modeling section are described in Table 4. The results of CTR modeling can be found in the previous work.[19]

Table 3. Specifications and Characteristics for Spherical Configuration

Parameter	First Reactor	Second Reactor	Third Reactor
Tube-side radius (m)	1.37	1.57	1.86
Shell-side radius (m)	1.57	1.77	2.06
Inlet temperature (K)	777	777	775
Catalyst distribution (wt %)	0.2	0.3	0.5
Membrane thickness (μm)	10	10	10
L/R	0.8	0.8	0.8
Minimum H_2/HC ratio	4.73	4.73	4.73
Membrane reactor radius (m)	1.37	1.57	1.86
Shell side radius (m)	1.42	1.62	1.91
Permeation side characteristic			
Inlet pressure (kPa)	1025	1780	1921
Inlet temperature (K)	777	768	766
Sweep gas composition (H_2)	0.695	0.738	0.761

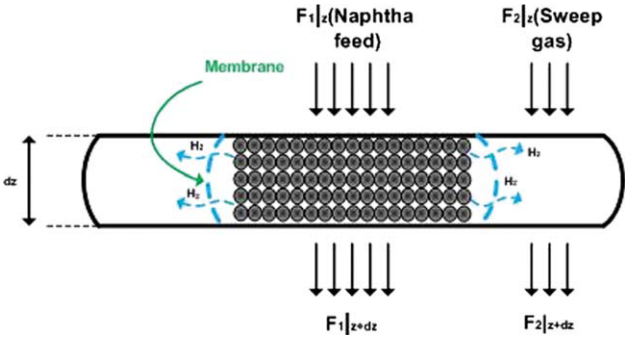

Figure 3. A computation element with the thickness of *dz*.

[Color figure can be viewed in the online issue, which is available at wileyonlinelibrary.com.]

Modeling assumptions

A 1-D model has been applied in this study. The following assumptions are made in the mathematical modeling of AF-SPBMR.

- A homogeneous catalytic packed bed (symmetric catalytic bed) is considered to lump the radial coordinate.
- Plug flow pattern is considered in the reactor.
- Axial heat and mass diffusion is neglected.
- Reactions take place on the catalyst particles.
- Hydrogen diffusion in the radial direction is negligible.
- Bed porosity is constant in axial and radial directions.
- Concentration and temperature are considered to be lumped in the radial direction.
- Intra-pellet heat and mass diffusion in catalyst pellet are neglected.
- Gases are assumed to be ideal.
- Heat loss is neglected (insulated outlet wall).

The following assumptions are made for the membrane layer:

- A supported membrane layer is used.
- Concentration polarization is negligible through the membrane layer and a lumped concentration is considered through the membrane.
- Membrane is a hydrogen perm-selective layer.
- Infinite selective membrane is considered.
- The Sievert's law is applicable.
- The effect of support is not considered on the membrane permeation rate.

Numerical Solution

To solve the set of equations, a two-stage procedure consisting of a steady-state stage followed by a dynamic stage has been applied. The initial condition for the dynamic stage is achieved by solving the equation of the steady-state stage. In the steady-state stage, all the time variants are set to zero and the catalyst activity is considered to be one. Thus, the results of the steady-state stage are used as the initial conditions for the time–integration of the dynamic state equations in each node through the reactor. The auxiliary correlations are presented in Appendix A.

Table 4. Mass and Energy Balance Equations for Axial-Flow Spherical Reactor

Fluid phase (Tube side)

$$D_{ej}\frac{1}{A_{c_1}}\frac{\partial}{\partial z}\left(A_{c_1}\frac{\partial C_j}{\partial z}\right)-\frac{1}{A_{c_1}}\frac{\partial(u_{z_1}A_{c_1}C_j)}{\partial z}+\rho_B a\sum_{i=1}^{m}v_{ij}r_i - \frac{A_p}{A_c}J_{H_2}=\varepsilon\frac{\partial C_j}{\partial t}\quad j=1,2,\ldots,n\ \ i=1,2,\ldots,m \tag{9}$$

$$k_{eff}\frac{1}{A_{c_1}}\frac{\partial}{\partial z}\left(A_{c_1}\frac{\partial T}{\partial z}\right)-\frac{1}{A_{c_1}}\frac{\partial}{\partial z}(\rho A_{c_1}u_{z_1}C_p(T-T_{ref})) - \left(\frac{A_p}{A_c}J_{H_2}C_p(T_{Shell}-T)\right)+\left(\frac{A_p}{A_c}U(T_{Shell}-T)\right) + \rho_B a\sum_{i=1}^{m}\Delta H_i r_i=\varepsilon\frac{\partial}{\partial t}(\rho C_p(T-T_{ref})) \tag{10}$$

Fluid phase (Shell side)

$$D_{ej}\frac{1}{A_{c_1}}\frac{\partial}{\partial z}\left(A_{c_1}\frac{\partial C_j}{\partial z}\right)-\frac{1}{A_{c_1}}\frac{\partial(u_{z_1}A_{c_1}C_j)}{\partial z} + \frac{A_p}{A_c}J_{H_2}=\varepsilon\frac{\partial C_j}{\partial t}\quad j=1,2,\ldots,n\ \ i=1,2,\ldots,m \tag{11}$$

$$k_{eff}\frac{1}{A_{c_1}}\frac{\partial}{\partial z}\left(A_{c_1}\frac{\partial T}{\partial z}\right)-\frac{1}{A_{c_1}}\frac{\partial}{\partial z}(\rho A_{c_1}u_{z_1}C_p(T-T_{ref})) + \left(\frac{A_p}{A_c}J_{H_2}C_p(T_{Shell}-T)\right)-\left(\frac{A_p}{A_c}U(T_{Shell}-T)\right)=\varepsilon\frac{\partial}{\partial t}(\rho C_p(T-T_{ref})) \tag{12}$$

Hydrogen permeation rate[38]

$$J_{H_2}=\frac{Q_0\exp(-\frac{E_{H_2}}{R_g T})}{\delta_{H_2}}(\sqrt{P_{H_2}^{tube}}-\sqrt{P_{H_2}^{Tube}})$$
$$Q_0=1.65\times10^{-5}\ \text{molm}^{-1}s^{-1}\text{kPa}^{\frac{-1}{2}},\ E_{H_2}=15.7\text{kjmol}^{-1} \tag{13}$$

Additional relations

$$A_c=\pi[R^2-(z-L_1)^2] \tag{14}$$

$$A_p=2\pi[R^2-(z-L_1)^2]^{0.5} \tag{15}$$

Boundary and initial conditions

$$z=0:\ C_j=C_{j0},\ \ T=T_0 \tag{16}$$

$$z=L_1+L_2\ :\ \frac{\partial C_j}{\partial z}=0,\ \ \frac{\partial T}{\partial z}=0 \tag{17}$$

$$t=0;C_j=C_j^{ss},\ T=T^{ss},\ T_s=T_s^{ss};\ a=1; \tag{18}$$

Ergun equation (pressure drop)

$$\frac{dP}{dz}=\frac{150\mu}{\phi_s^2 d_p^2}\frac{(1-\varepsilon)^2}{\varepsilon^3}\frac{Q}{A_c}+\frac{1.75\rho}{\phi_s d_p}\frac{(1-\varepsilon)}{\varepsilon^3}\frac{Q^2}{A_c^2} \tag{19}$$

Catalyst deactivation

$$\frac{da}{dt}=-K_d\exp\left(-\frac{E_d}{R_g}\left(\frac{1}{T}-\frac{1}{T_R}\right)\right)a^7$$
$$T_R=770\text{K},E_d=1.642\times10^5\text{jmol}^{-1},\ K_d=5.926\times10^{-5}h^{-1} \tag{20}$$

Table 5. Comparison Between Predicted Production Rate and Plant Data (Unsteady-State Model Validation)

Time (day)	Naphtha Feed (ton/h)	Plant (kmol/h)	Tubular (kmol/h)	Deviation %: 100*(Tubular-Plant)/Plant	Spherical (kmol/h)
0	30.41	225.90	221.5802	−1.91	219.2983
34	30.41	224.25	222.5122	−0.77	220.2618
62	31.00	229.65	227.9313	−0.75	225.7263
97	30.78	229.65	226.7749	−1.25	224.5911
125	31.22	229.65	230.7985	+0.50	228.6526
160	31.22	229.65	231.2730	+0.71	229.1520
188	28.55	211.60	209.8377	−0.83	207.6284
223	30.33	222.75	224.7191	+0.88	222.6013
243	31.22	233.05	232.1821	−0.37	230.1117
298	30.67	228.65	228.1752	−0.21	226.1110
321	30.76	227.64	229.0932	+0.64	227.0446
398	42.35	317.30	324.5555	+2.28	323.0820
425	42.32	317.94	324.4826	+2.05	323.0228
461	42.32	317.94	324.6987	+2.12	323.2582
490	42.32	317.94	324.8622	+2.17	323.4366
524	42.32	313.09	325.0433	+3.81	323.6341
567	42.54	317.94	327.0586	+2.86	325.6805
610	42.54	313.90	327.2581	+4.25	325.8980
717	37.86	286.15	289.3742	+1.12	287.8223
771	38.51	282.10	294.9026	+4.53	293.4003

This set of equations is solved by means of the orthogonal collocation method.[39,40] The orthogonal collocation method is presented in Appendix B. The system of PDEs is transformed into an ordinary differential equation (ODE) system by means of the orthogonal collocation method. Energy and mass balance equations are developed for each point. The system of ODEs is integrated by a modified second-order Rosenbrock formula. It is noted that this method is well suited for systems of stiff equations.[41]

Model Validation

Dynamic model validation

The validity of the mentioned model has been checked by comparing the applied data with the observed experimental data[42] of the industrial packed-bed reactor over 800 operation days. The predicted results of the production rate, the corresponding observed data, and the residual error are presented in Table 5. Acceptable agreements are observed between the daily plant data and simulation results, thus this model can successfully satisfy the industrial conditions. According to the reported results, the deviation is observed from the reported plant values. It is due to underestimating the actual kinetics and reaction rate of naphtha reforming.

Steady-state model validation

Table 6 demonstrates the plant data for CTR and predicted mole fractions of components at the output of the system for the steady-state condition. Analyses of components (paraffin, olefins, naphthene, and aromatic) are performed by PONA Test in Stan Hop Seta apparatus. The aromatic is tested specially by ASTM 2159 equivalent to UOP 273 method.[42]

Results and Discussions

To find a proper number of interior collocation points which provide satisfactory results, the temperature of the first reactor is plotted vs. the mass of catalyst for different interior collocation points in Figure 4. In Figure 4a, 1, 2, and 3 as well as, in Figure 4b, 1, 5, and 7 interior collocation points have been used, respectively. As it is shown in Figure 4a, when the number of interior collocation points is not enough, the diversity appears between the curves. However, by increasing the number of interior collocation points (Figure 4b), the discrepancy between the

Table 6. Comparison Between Model Prediction and Plant Data for Fresh Catalyst (Steady-State Model Validation)

Reactor No.	Inlet Temperature (K)	Inlet Pressure (kPa)	Catalyst Distribution (wt %)	Input Feedstock (mol %)	
1	777	3703	20	Paraffin	49.3
2	777	3537	30	Naphthene	36
3	775	3401	50	Aromatic	14.7

	Outlet temperature (K)			Aromatic in reformate (mol %)		
	Plant	CTR	SMR	Plant	CTR	SMR
1	722	727.3	727.8	–	34.67	35.15
2	753	751.0	751.2	–	47.19	47.73
3	770	770.5	769.7	57.70	56.18	57.67

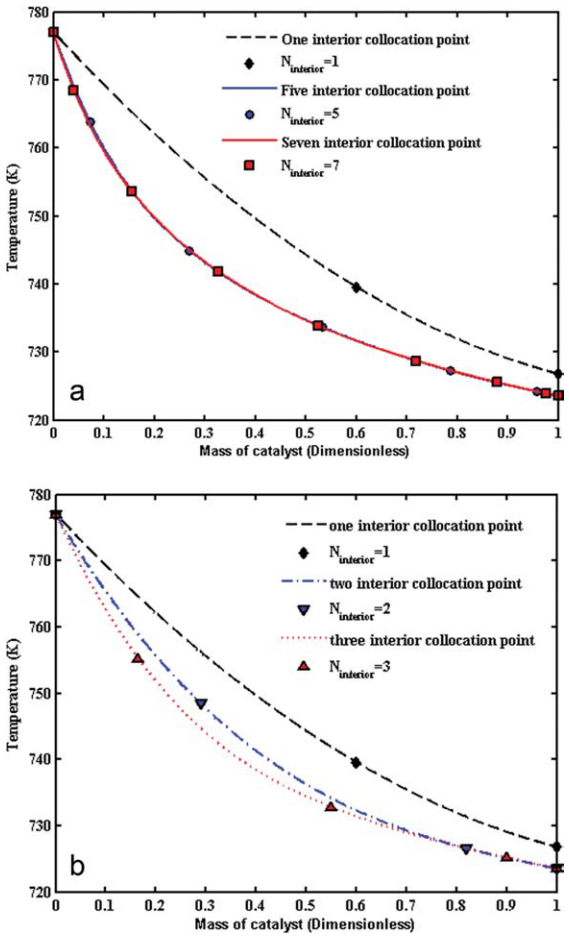

Figure 4. The temperature of the first reactor vs. the mass of catalyst (a) with 1, 2, and 3 as well as (b) 1, 5, and 7 interior orthogonal collocation points.

[Color figure can be viewed in the online issue, which is available at wileyonlinelibrary.com.]

curves disappears. The curves with 5 and 7 interior points cover each other thoroughly. Therefore, the $N = 5$ is the most accurate choice.

The hydrogen molar flow rate along AF-SPBR is depicted in Figure 5. As it can be seen, the hydrogen molar flow rate increases along the first and the second reactors. The smaller graph in Figure 5 magnifies the hydrogen molar flow rate in the third reactor. The hydrogen production rate increases gradually, reaches its maximum and then decreases in the third reactor due to equilibrium limitations. In other words, hydrogen is consumed in the third reactor and its molar flow rate decreases. Consequently, the idea of using the membrane layer is a proper suggestion.

The effect of L/R *ratio*

The effect of L/R ratios on the pressure is an important issue. The effect of different L/R ratios on the pressure vs. the mass of catalyst is depicted in Figure 6a. The pressure drop increases suddenly at the inlet and the outlet of the reactor due to smaller cross-sectional area at these points. As proceeding along the reactor, the cross-sectional area increases gradually and the pressure drop becomes approximately constant. Consequently, the location of perforated screens can be adjusted to reach the desired pressure drop. The Ergun equation justifies all these observations. Figure 6b shows the effects of different L/R ratios on the H_2/HC molar ratio. In lower L/R ratios, less area of the inner sphere is coated by a membrane layer. Thus, it causes lower hydrogen permeation rate and higher H_2/HC molar ratio. It is recommended to maintain H_2/HC molar ratio in the range of 4–6 Ref. 42 in naphtha reforming process to reduce coking and prevent a huge load on the catalyst during the operation. The inlet H_2/HC molar ratio to the first reactor equals 4.73 in CTR; however, it will not be allowed to fall below this ratio during the recent study by adjusting the permeation pressure. The $L/R = 0.9$ has the best H_2/HC molar ratio however the pressure drop is unacceptably high. Proper ratio can shift the reaction to hydrogen and aromatic production, whereas it may reduce the pressure drop through the reactor. Therefore, it is not economical to work in this L/R ratio because of high operating costs. On the other hand, working at $L/R = 0.5$ is not logical because most of the reactor space is empty without any catalyst. According to these criteria, the $L/R = 0.8$ is a proper choice. The related permeation pressures (by considering $L/R = 0.8$) which keep the H_2/HC molar ratio at a minimum value of 4.73 and higher in all three reactors are 1025, 1780, and 1921 kPa, respectively.

A comparison between CTR and AF-SPBMR configurations

The H_2/HC molar ratio vs. the mass of catalyst for CTR and spherical membrane reactor (SMR) is shown in Figure 7a. The H_2/HC molar ratio increases along CTR due to continuous hydrogen production; however, its variation is limited along SMR. The hydrogen production rate is higher than its permeation rate at the entrance of each reactor in SMR, mainly due to its higher temperature, which causes increasing/decreasing trends (maximum point). The molecular weight vs. the mass of catalyst for CTR and SMR is illustrated in Figure 7b. As it can be seen, the molecular

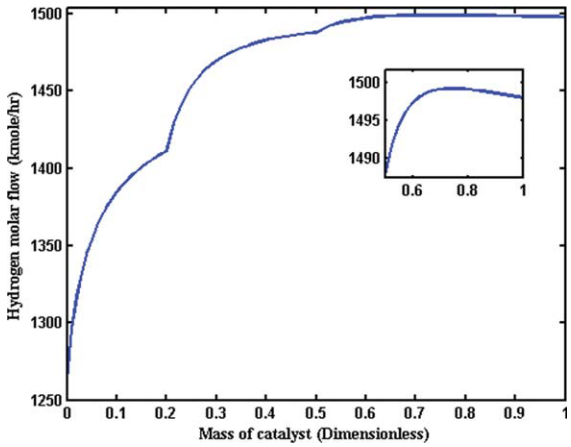

Figure 5. Hydrogen molar flow rate along AF-SPBR.

[Color figure can be viewed in the online issue, which is available at wileyonlinelibrary.com.]

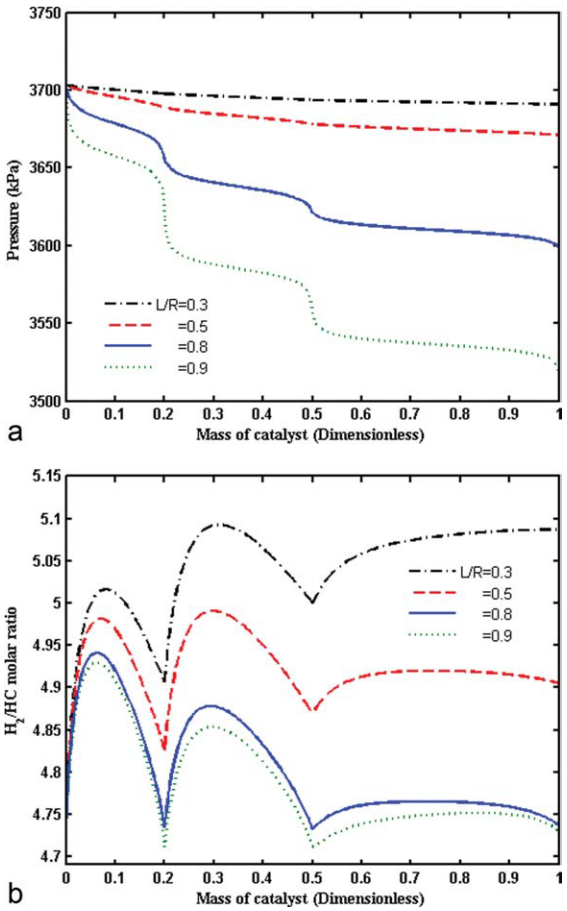

Figure 6. The effect of different *L/R* ratios on (a) pressure and (b) the H_2/HC molar ratio, vs. the mass of catalyst.

[Color figure can be viewed in the online issue, which is available at wileyonlinelibrary.com.]

weight decreases along the CTR configuration as it can be expected. Heavy molecules are cracked and smaller molecules are formed during the naphtha reforming process. Because of the hydrogen removal from the tube side of SMR, the average molecular weight increases. In fact, hydrogen is the lightest component in naphtha reforming process. The minimums in the molecular weight are exactly proportional to the maximums in Figure 7a. Higher H_2/HC molar ratio leads to higher hydrogen content and lower average molecular weight.

The aromatic molar flow rate vs. the mass of catalyst for CTR and SMR is demonstrated in Figure 8a. The aromatic yield increases in SMR in comparison with the one in CTR. Considering the small graph shown in Figure 8a, the aromatic yield increases with the rate of 3 kmol/h in SMR which results in a very large amount per year. The total hydrogen production rate for CTR and SMR is depicted in Figure 8b. The total hydrogen production rate increases with the rate of 5 kmol/h. Considering the small graph shown in Figure 8b, using membrane can satisfy the anticipated results and solve the problem of undesirable hydrogen consumption in the third reactor according to the Le Chatelier's principle. The hydrogen production rate does not decrease in SMR. In fact, this parameter increases as it can be seen in Figure 8b. Molar flow rates of reactants and products vs. the mass of catalyst for CTR and SMR are illustrated in Figure 8c. Naphthene and paraffin consumption rates in SMR are higher compared with CTR. Also, the light ends are produced more in SMR. The main reactions in the third reactor are light end reactions. Most of the off gases (light ends) are produced by the paraffin consumption (compare the graphs of paraffin and light ends). In other words, the light ends production rate is strongly affected by temperature. Therefore, a majority of light ends are produced in the third reactor, which has the highest temperature profile. Each break point in these figures indicates the inlet temperature of the following reactor. As temperature is increased by applying preheaters at the inlet of each reactor, the reaction rates change and discontinuities appear in the figure.

The pressure profiles are illustrated in Figure 9. At $L/R = 0.8$, the pressure drop in SMR is considerably lower than the one in CTR. The sudden changes in the pressure profile of SMR (as clearly shown in Figure 6a) are related to the inlet and the outlet points of each reactor. At these points, higher

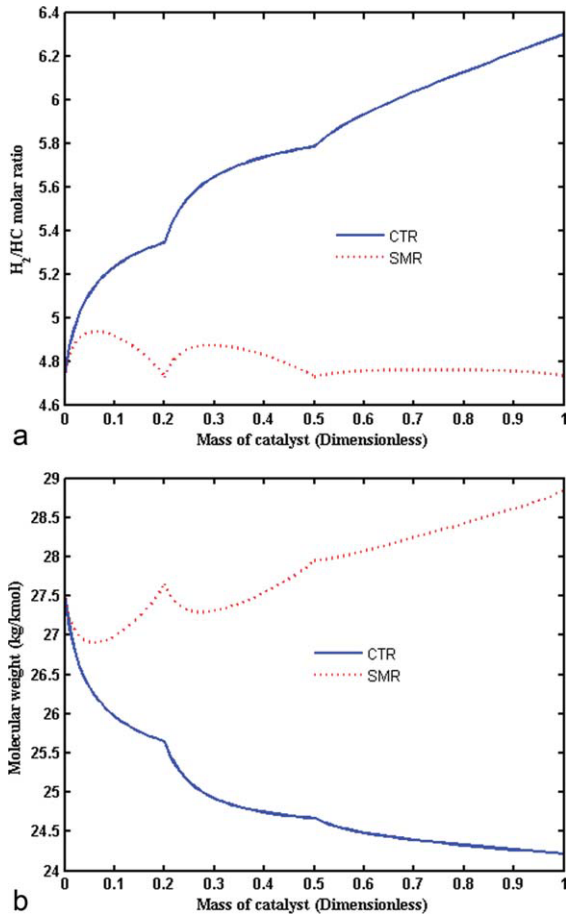

Figure 7. (a) The H_2/HC molar ratio and (b) the molecular weight, vs. the mass of catalyst for CTR and SMR.

[Color figure can be viewed in the online issue, which is available at wileyonlinelibrary.com.]

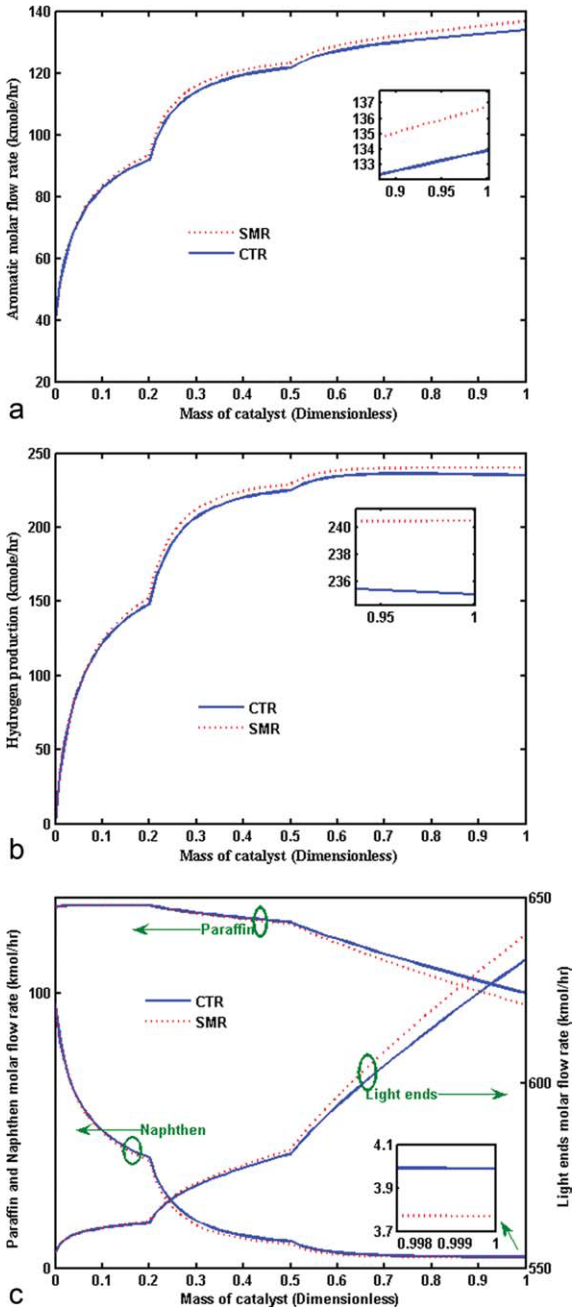

Figure 8. (a) The aromatic molar flow rate, (b) the total hydrogen production, and (c) naphthene and paraffin and light ends, vs. the mass of the catalyst for CTR and SMR.

[Color figure can be viewed in the online issue, which is available at wileyonlinelibrary.com.]

pressure drop is encountered due to huge amount of fluid entering and leaving small inlet and outlet zones.

The temperature profile of the reaction side for CTR and SMR is illustrated in Figure 10a. Trend of temperatures are similar in both configurations. As previously mentioned, the naphtha reforming reactions are highly endothermic. Thus, the temperature decreases along the reactors. The dehydrogenation reaction (Eq. 1) in the first reactor results in a considerable decrease in the temperature of the first reactor. The catalyst activity of both configurations is plotted in Figure 10b. According to the catalyst deactivation rate (Eq. 20), the catalyst activity has a reverse relationship with the temperature. Therefore, the third reactor with the highest temperature profile (see Figure 10a) has the lowest catalyst activity. Because of a decrease in the temperature along the reactor, the catalyst activity rises as proceeding along the reactors.

Permeation side

The sweeping gas temperature profile is shown in Figure 11a. The sweeping gas inlet temperature is considered to be 777 K the same as the inlet naphtha feed temperature enters the first reactor. The sweeping gas temperature decreases due to its heat exchange with the tube side. In other words, the sweeping gas provides a heat source for the reaction side of the first and the second reactors. The temperature profile of the third reactor (Dimensionless axial position: 0.5–1) clarifies that the parallel flow of the sweeping gas could possibly be more effective to increase the aromatic production rate. Here, the undesired heat transfer from the reaction side leads to an increase in the sweeping gas temperature.

The average molecular weight and the hydrogen mole fraction along the shell sides are illustrated in Figure 11b. The molecular weight of the sweeping gas decreases along the reactor due to the hydrogen permeation from the reaction side to the shell side. The hydrogen mole fraction increases from 0.69 to 0.78.

The effect of time

Time is an important parameter which is considered in the following 3-D graphs. The catalyst is deactivated in the course of time. As it can be seen in Figure 12a, at the entrance of the first reactor, the catalyst activity is lower compared with the other parts due to higher gas temperature at the entrance of the reactor. A contour plot of the catalyst

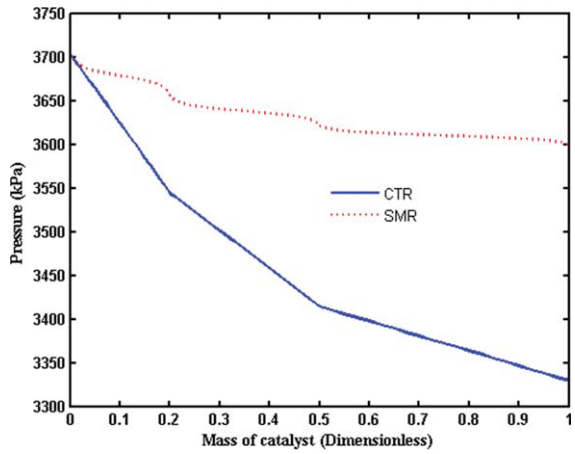

Figure 9. The pressure profile vs. the mass of catalyst for CTR and SMR.

[Color figure can be viewed in the online issue, which is available at wileyonlinelibrary.com.]

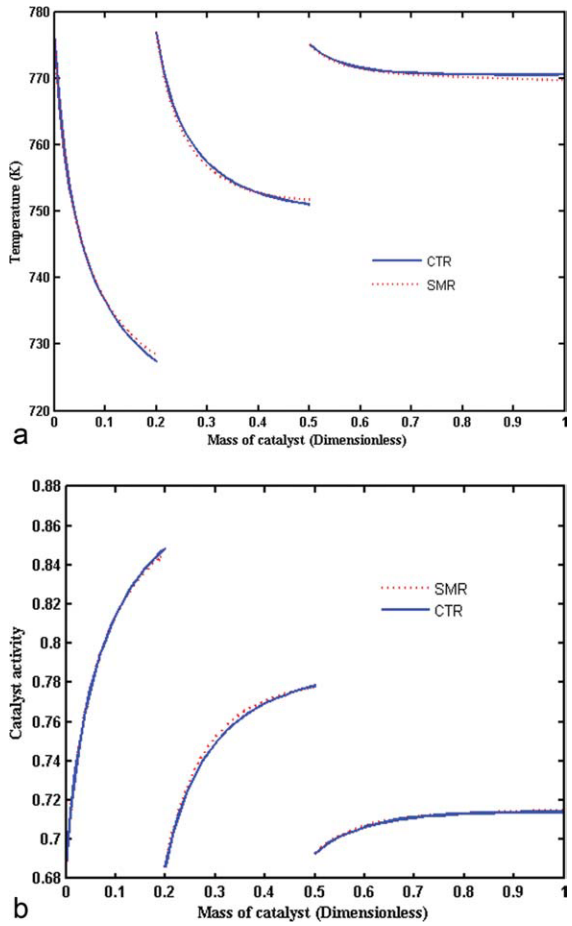

Figure 10. (a) The temperature profile and (b) the catalyst activity, vs. the mass of catalyst for CTR and SMR.

[Color figure can be viewed in the online issue, which is available at wileyonlinelibrary.com.]

activity in the first reactor is provided in Figure 12b to show the effect of temperature on the catalyst lifetime. As previously mentioned, higher catalyst activity along the reactor in each specific time can be justified by the temperature profile of the reactor. Similarly, the catalyst activity of the second reactor decreases as time goes on (Figure 12c). The catalyst activity of the third reactor is the least (Figure 12d) due to higher temperature profile of the third reactor in comparison with the first and second reactors.

The reaction rates decrease as the catalyst activity decreases. Thus, a decrease in the production rates and an increase in the reactant rates are anticipated as time goes on. To investigate the deduction, the reactants and products molar flow rates as functions of time and the length of the third reactor are depicted in the following graphs. Because of the catalyst deactivation, the paraffin molar flow rate (unreacted paraffin) increases with time (see Figure 13a). Because paraffin is a reactant, its molar flow rate decreases along the third reactor. The same trend is observed for naphthene molar flow rate (see Figure 13b). The naphthene molar flow rate decreases along the reactor, however, it increases in the course of time.

The aromatic molar flow rate vs. time and the length of the third reactor is depicted in Figure 14a. The aromatic molar flow rate decreases in the course of time, however, it increases along the third reactor. At any intersection of three reactors in Figure 14b, the light ends molar flow rate decreases with time mainly due to catalyst deactivation (dynamic situation). Figure 14c shows the total hydrogen production rate. Hydrogen has a dual role in naphtha reforming reactions, i.e., it acts in the first reaction as a product and simultaneously in the second, the third, and the fourth reactions as a reactant. The hydrogen production and consumption rates (by reactions no. 1 3, and 4, respectively) decrease in the course of time due to the catalyst deactivation. However in SMR, the decrement in hydrogen consumption prevails over the decrement in its production which leads to a slight increase in hydrogen production rate with time.

The effect of flow ratio augmentation

One of the advantages of Sphs is that the flow rate can be increased without any sever pressure drop. The pressure

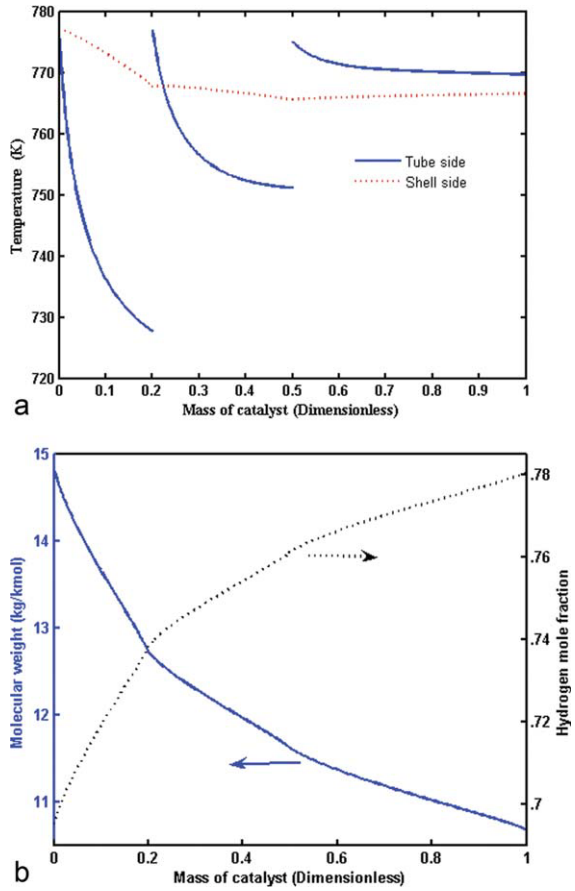

Figure 11. (a) The sweeping gas temperature profile and (b) the molecular weight of the sweeping gas and the hydrogen mole fraction, vs. the mass of catalyst.

[Color figure can be viewed in the online issue, which is available at wileyonlinelibrary.com.]

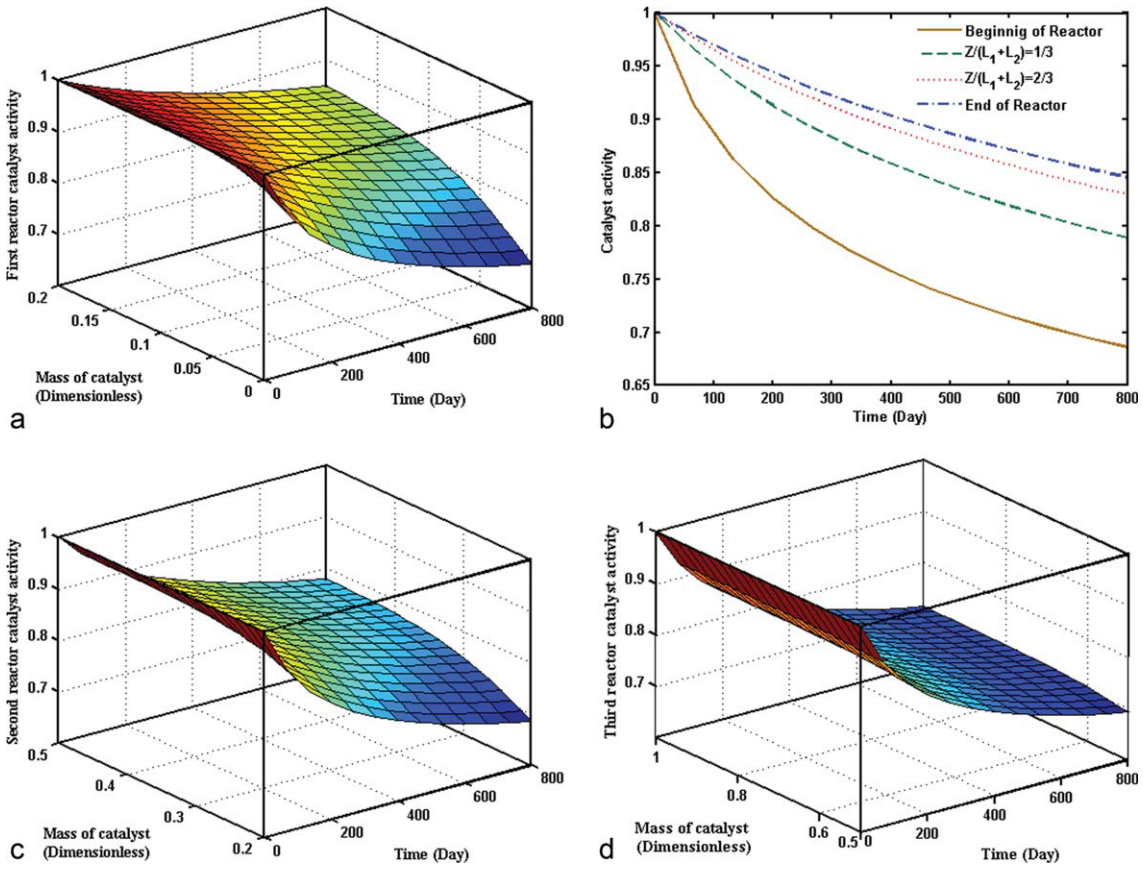

Figure 12. (a) Catalyst activity vs. time and the length of the first reactor, (b) a contour plot for catalyst activity in the first reactor, (c) the catalyst activity vs. time and the length of the second reactor, and (d) catalyst activity vs. time and the length of the third reactor.

[Color figure can be viewed in the online issue, which is available at wileyonlinelibrary.com.]

drop in Sphs is less than the one in tubs. The effect of flow scale up ratio (FR) on the pressure, hydrogen, and the aromatic yield is taken into consideration. FR compares the feed stream of the spherical configuration with the tubular one. The effect of various FRs on the outlet pressure of the third reactor of CTR and SMR are compared in Figure 15a. The prediction of the behavior of naphtha reactions is too complicated. Even a small change in the inlet conditions of the first reactor can significantly affect the reactions and the trends in all reactors. At low flow ratios (i.e., FR = 0.1), the aromatic yield increases along the first and the second reactors; however, it decreases along the third reactor. The further increase in the feed molar flow rate increases the aromatic production. For higher FRs, the pressure drop as well as lower residence time, reduces the products yield in CTR. SMR has the potential to increase the products yield by the hydrogen removal from the reaction side. Consequently, the aromatic yield in SMR is more than the one in CTR for different FRs (Figure 15b). It is not possible to increase the feed flow ratio of CTR more than 2.5; however, it can be increased to even more than 4 for SMR. The effect of the FR on the hydrogen yield for CTR and SMR is illustrated in Figure 15c. Higher hydrogen yield is observed as the FR ratio increases. When FR is low, a part of hydrogen turns into light ends via the third and fourth reactions in the third reactor and the hydrogen amount decreases due to higher temperature of the third reactor. In a specific range of FR, lower residence time of reactants in the catalytic bed acts against the above mentioned issue (simultaneous FR and hydrogen increase), and the change in hydrogen yield is negligible. Moreover, the products yield decreases at high flow ratios due to the pressure drop and lower residence time. Assisting membrane in SMR configuration acts properly and partially compensates this problem.

The definition for hydrogen and the aromatic yields is as follows:

$$Y_i = \frac{F_i}{F_{\text{Paraffine}} + F_{\text{Naphthene}} + F_{\text{Aromatic}}} \tag{21}$$

where i denotes hydrogen or aromatic.

The preceding plots show the superiority of AF-SPBMR to the conventional one. Also, they can be beneficial during the operation.

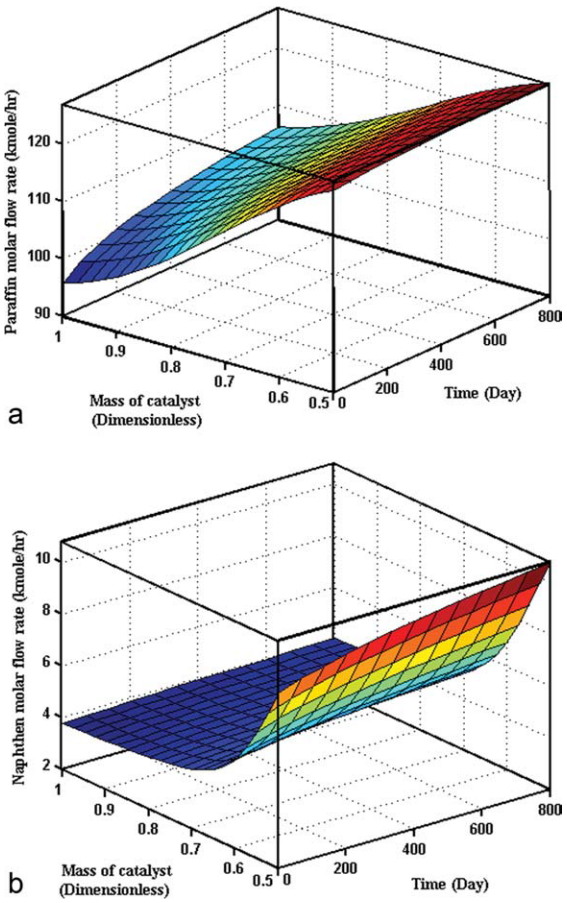

Figure 13. (a) The paraffin molar flow rate and (b) the naphthen molar flow rate, vs. time and the length of the third reactor.

[Color figure can be viewed in the online issue, which is available at wileyonlinelibrary.com.]

Optimization (DE Algorithm)

The decrease in products yield and the increase in productivity are observed owing to flow ratio augmentation. When the flow ratio increases, the products yield decrease as a result of a reduction in the residence time and predominantly the reaction rates. The solution to this unfavorable observation is achieved by optimization techniques. Some decision variables are identified, which can affect the aromatic and hydrogen yields. The most important decision variables are the inlet feed temperature, the sweeping gas pressure, the sweeping gas temperature, and the sweeping gas mole fraction. A case study is taken into consideration to imply the performance of these parameters on the products yield by the optimization techniques. Therefore, it is explained how to adjust the decision parameters to achieve the same yield similar to the case of no flow scale up ratio (FR = 1). The optimized parameters for a number of FRs are explained in Table 7. In fact, the variables adjust the circumstances in a way that the same results are achieved as before when the flow ratio has been changed. For the last two flow ratios (FR = 2.5 and FR = 3), 13% and 42% increases are considered in the amount of catalysts in reactors during the optimization step.

The corresponding optimized results for hydrogen and aromatic productions before and after the flow scale up ratios (FR = 2) are presented in Figures 16a, b. A brief description on the DE algorithm is given in Appendix C.

These kinds of data can be beneficial during the field operation in the process control unit.

Conclusions

AF-SPBMR has been proposed as a novel configuration for catalytic naphtha reforming process. The performance of

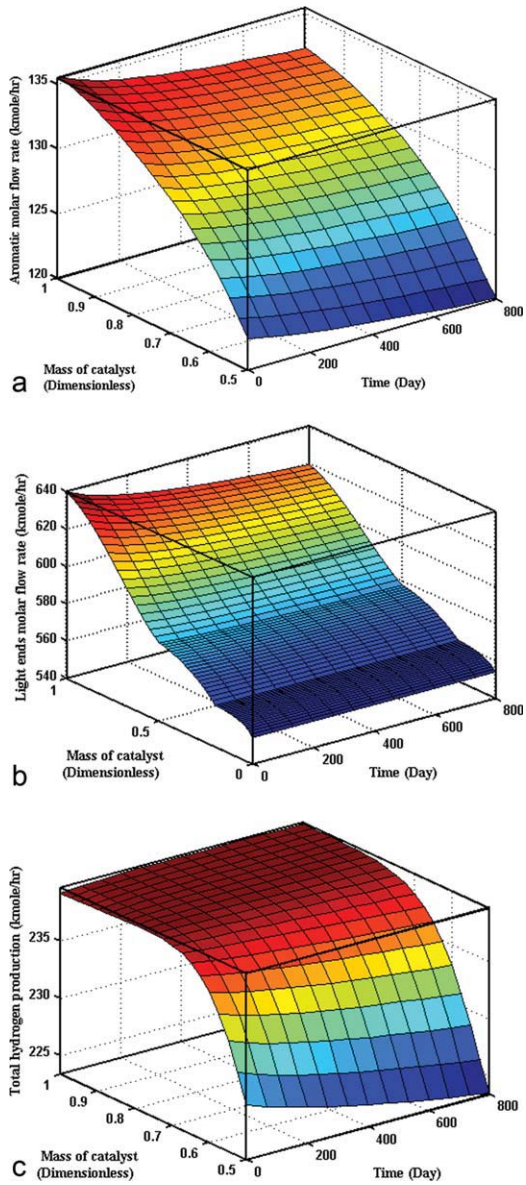

Figure 14. (a) The aromatic molar flow rate, (b) the light ends molar flow rate, and (c) the total hydrogen production rate vs. time and the length of the third reactor.

[Color figure can be viewed in the online issue, which is available at wileyonlinelibrary.com.]

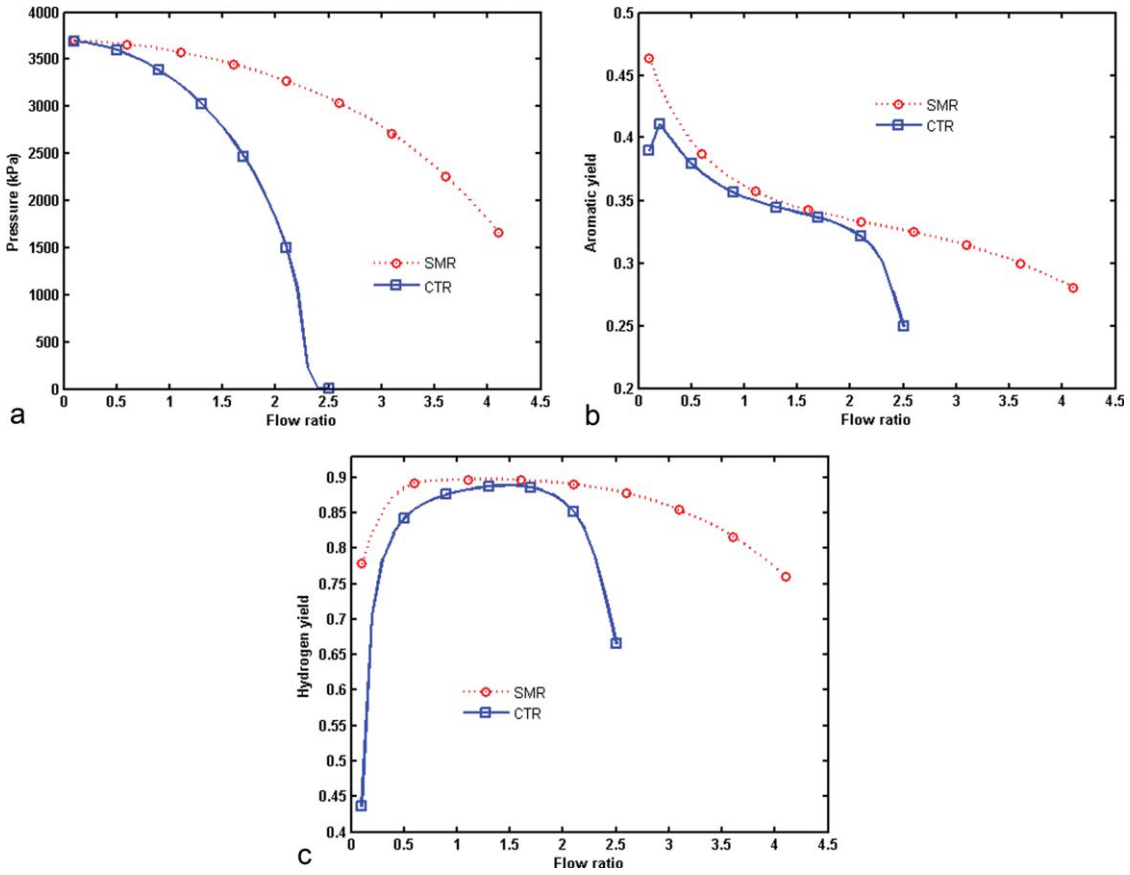

Figure 15. The effect of flow ratio on (a) the outlet pressure of the third reactor, (b) the aromatic yield, and (c) the hydrogen yield, for CTR and SMR.

[Color figure can be viewed in the online issue, which is available at wileyonlinelibrary.com.]

these Sphs with the axial-flow pattern has been investigated in this manuscript. Membrane technology is assisted in this configuration to enhance the aromatic production and produce pure hydrogen as an important chemical feed stock. Because higher flow rate of feed can be introduced in Sphs, some decision variables have been determined by DE optimization method to compensate the decrease in the aromatic yield caused by the flow ratio augmentation. Although the operational performance of such a new configuration is unknown and there are numerous problems before commercialization, such a theoretical investigation provides a proper primary foresight about the operation of new reactor. The experiments can be carried out in conjunction with the mathematical modeling to improve the predicted results of the model and become a powerful tool for designing new plants.

Table 7. The Obtained Results for Optimization (DE) Section

Reactor No.	Inlet Temperature of Reaction Side (K)	Sweep Gas Pressure (kPa)	Sweep Gas Temperature (K)	Sweep Gas Composition (% H_2)	Catalyst Scale-Up Ratio
Flow scale up ratio (FR = 1.5)					
First reactor	781.649	595.379	792.324	0.696	1.000
Second reactor	784.586	1192.779	–	–	1.000
Third reactor	781.258	1455.297	–	–	1.000
Flow scale up ratio (FR = 2)					
First reactor	781.488	377.256	780.903	0.683	1.000
Second reactor	780.754	1135.830	–	–	1.000
Third reactor	791.926	913.552	–	–	1.000
Flow scale up ratio (FR = 2.5)					
First reactor	777.419	408.122	799.800	0.659	1.134
Second reactor	784.899	607.0159	–	–	1.134
Third reactor	788.899	590.467	–	–	1.134
Flow scale up ratio (FR = 3)					
First reactor	777.687	484.510	786.118	0.652	1.427
Second reactor	786.439	719.755	–	–	1.427
Third reactor	796.549	490.410	–	–	1.427

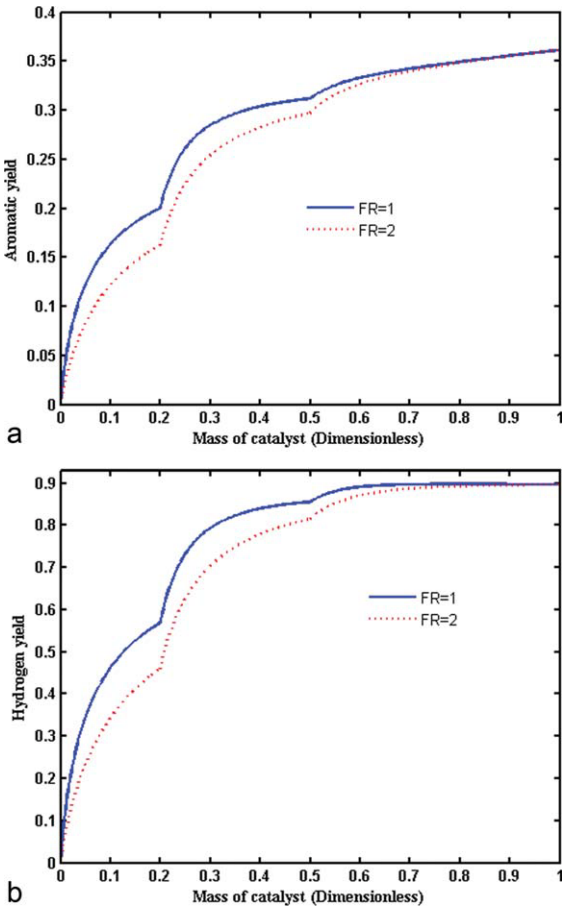

Figure 16. The results of running program with the optimized parameters for FR = 2 on (a) aromatic yield and (b) hydrogen yield.

[Color figure can be viewed in the online issue, which is available at wileyonlinelibrary.com.]

Notation

a = catalyst activity
a_{ij} = element of matrix A
A = moles of aromatic formed (kmol h^{-1})
A = matrix defined in Eq. B12
A_c = cross section between the inner and the outer sphere (m^2)
A_{c_1} = cross-section area of catalytic packed-bed reactor (inner sphere) (m^2)
A_p = perimeter area of the inner sphere (m)
B = matrix is defined in Eq. B12
b_{ij} = element of matrix B
C_j = concentration of component j (kmol m^{-3})
C_i = coefficient of Eqs. A1 and A2
C_{j0} = inlet concentration of component j (kmol m^{-3})
C_p = specific heat capacity (kJ $kmol^{-1}$ K^{-1})
d_p = particle diameter (m)
D_{e_j} = effective diffusivity of component j (m^2 s^{-1})
D_{im} = diffusivity of component i in the gas mixture (m^2 s^{-1})
E_d = activation energy of catalyst (J mol^{-1})
E_i = activation energy for ith reaction, (kJ $kmol^{-1}$)
h_f = heat-transfer coefficient (W m^{-2} K^{-1})
HC = hydrocarbon molar flow rate (kmol h^{-1})
H_2 = hydrogen (kmol h^{-1})
J = Jacobi function
k_{eff} = effective thermal conductivity (W m^{-1} s^{-1})
k_{c_i} = mass-transfer coefficient for component i (m h^{-1})
k_{f_1} = forward rate constant for reaction (1) (kmol h^{-1} $kgcat^{-1}$ MPa^{-1})
k_{f_2} = forward rate constant for reaction (2) (kmol h^{-1} $kgcat^{-1}$ MPa^{-2})
k_{f_3} = forward rate constant for reactions (3) (kmol h^{-1} $kgcat^{-1}$)
k_{f_4} = forward rate constant for reactions (4) (kmol h^{-1} $kgcat^{-1}$)
K_{e_1} = equilibrium constant (MPa^3)
K_{e_2} = equilibrium constant (MPa^{-1})
K_d = deactivation constant of the catalyst (h^{-1})
L = length of reactor (m)
l_j = building block of Jacobi polynomial
m = number of reaction
m_c = mass of catalyst (kg)
M_i = molecular weight of component i (kg $kmol^{-1}$)
M_w = average molecular weight of the feedstock (kg $kmol^{-1}$)
n = average carbon number for naphtha
n = number of component
N = degree of Jacobi function
N_A = molar flow rate of aromatic (kmol h^{-1})
N_i = molar flow rate of component i (kmol h^{-1})
p = moles of paraffin formed (kmol h^{-1})
P_i = partial pressure of ith component (kPa)
P = total pressure (kPa)
Q = volumetric flow rate (m^3 s^{-1})
R = radius (m)
r_i = rate of reaction for ith reaction (kmol $kgcat^{-1}$ h^{-1})
R_g = gas constant (kJ $kmol^{-1}$ K^{-1})
s_a = specific surface area of catalyst pellet (m^2 kg^{-1})
t = time (h)
T = temperature of gas phase (K)
T_{ref} = reference temperature (K)
T_R = reference temperature (K)
u_z = axial velocity (m s^{-1})
x = variable represent length of reactor (m)
y_N = Jacobi polynomial of degree (N)
y_i = mole fraction for ith component in gas phase
y_{i_s} = mole fraction for ith component on solid phase
v_c = critical volume (cm^3 $kmol^{-1}$)
y'_N = first derivative of Jacobi equation
y_N = second derivative of Jacobi equation

Greek letters

α = characteristic parameter of Jacobin equation
β = characteristic parameter of Jacobin equation
γ = coefficient of Eq. A1
ε = void fraction of catalyst bed
μ = viscosity of gas phase (kg m^{-1} s^{-1})
v_{i_j} = stoichiometric coefficient of component i in reaction j
ρ = density of gas phase (kg m^{-3})
ρ_B = catalyst bulk density (kg m^{-3})
σ = tensile stress (Nm^{-2})
ϕ_s = sphericity
ΔH = heat of reaction (kJ $kmol^{-1}$ of H_2)

Subscripts

a = aromatic
h = hydrogen
i = numerator for reaction
j = numerator for component
n = naphthene
out = outlet
p = paraffin
ss = steady state
T = transpose

Abbreviations

AF-SPBMR = axial flow spherical packed-bed membrane reactor
CTR = conventional tubular reactor
FBP = final boiling pint (°C)

IBP = initial boiling pint (°C)
L.E = Light ends
LHSV = liquid hourly space velocity (h^{-1})
OF = objective function
Pt = platinum
Re = rhenium
RON = research octane number
SMR = spherical membrane reactor
Sph = spherical reactor
tub = tubular reactor
TBP = true boiling point (K)
WHSV = weight hourly space velocity (h^{-1})

Literature Cited

1. Antos GA, Aitani AM. *Catalytic Naphtha Reforming*, 2nd ed. New York: Marcel Dekker Inc.,1995.
2. Ali MA, Ali SA, Siddiqui MAB. An appraisal of hydrocarbons conversion reactions during naphtha reforming process. *Petrol Sci Technol*. 2007;25:1321–1331.
3. Hu Y, Xu W, Chu HSJ. A dynamic model for naphtha catalytic reformers. In: *International Conference on Control Applications*. Taipei, Taiwan, September 2-4 2004.
4. Smith RB. Kinetic analysis of naphtha reforming with platinum catalyst. *Chem Eng Progress*. 1959;55:76–80.
5. Weifeng H, Hongye S, Yongyou H, Jian C. Lumped kinetics model and its on-line application to commercial catalytic naphtha reforming process. *J Chem Ind Eng*. 2006;57:1605–1611.
6. Stijepovic MZ, Ostojic AV, Milenkovic I, Linke P. Development of a kinetic model for catalytic reforming of naphtha and parameter estimation using industrial plant data. *Energy Fuels* 2009;23:979–983.
7. Ramage MP, Graziani KP, Krambeck FJ. 6 Development of mobil's kinetic reforming model. *Chem Eng Sci*. 1980;35:41–48.
8. Ramage MP, Graziani KR, Schipper PH, Krambeck FJ, Choi BC. A review of mobil's industrial process modeling philosophy. *Adv Chem Eng*. 1987;13:193–266.
9. Krane HG, Groh AB, Schuhnan BL, Sinfeh JH. Reactions in catalytic reforming of naphthas. In: *5th World Petroleum Congress*, New York, May 30 - June 5, 1959.
10. Kmak WS. A kinetic simulation model of the powerformmg process. AIChE Meeting, Houston, TX. 1972.
11. Marin GB, Froment GF, Lerou JJ, Backer WD. Simulation of a catalytic naphtha reforming unit W. *Eur Fed Chem Eng*. 1983;2:1–7.
12. Juarez JA, Macias EV. Kinetic modeling of naphtha catalytic reforming reactions. *Energy Fuels* 2000;14:1032–1037.
13. Li J, Tan Y, Liao L. Modeling and optimization of a semi-regenerative catalytic naphtha reformer. In: *Proceedings of the 2005 IEEE Conference on Control Applications*. Toronto, Canada, August 28-31 2005.
14. Mostafazadeh AK, Rahimpour MR. A membrane catalytic bed concept for naphtha reforming in the presence of catalyst deactivation. *Chem Eng Process*. 2009;48:683–694.
15. Weifeng H, Hongye S, Shengjing M, Jian C. Multiobjective optimization of the industrial naphtha catalytic reforming process. *Chin J Chem Eng*. 2007;15:75–80.
16. Rahimpour MR. Enhancement of hydrogen production in a novel fluidized-bed membrane reactor for naphtha reforming. *Int J Hydrogen Energy* 2009;34:2235–2251.
17. Taskar U, Riggs JB. Modeling and optimization of a semi regenerative catalytic naphtha reformer. *AIChE J*. 1997;43:740–753.
18. Juarez JA, Macias EV, Garcia LD, Arredondo EG. Modeling and simulation of four catalytic reactors in series for naphtha reforming. *Energy Fuels* 2001;15:887–893.
19. Iranshahi D, Rahimpour MR, Asgari A. A novel dynamic radial-flow, spherical-bed reactor concept for naphtha reforming in the presence of catalyst deactivation. *Int J Hydrogen Energy*. 2101;35: 6261–6275.
20. Pieck CL, Sad MR, Parera JM. Chlorination of Pt-Re/A1203 during naphtha reforming. *J Chem Technol Biotechnol*. 1996;67:61–66.
21. Martin N, Viniegra M, Zarate R. Coke characterization for an industrial Pt–Sn/g-Al_2O_3 reforming catalyst. *Catal Today*. 2005; 107–108:719–725.
22. Ren XH, Bertmer M, Stapf S, Demco DE, Blümich B, Kern C, Jess A. Deactivation and regeneration of a naphtha reforming catalyst. *Appl Catal A*. 2002;228:39–52.
23. Borgna A, Garetto TF, Monzon M, Apesteguia CR. Deactivation model with residual activity to study thioresistance and thiotolerance of naphtha reforming catalyst. *J Catal*. 1994;146:69–81.
24. Viswanadham N, Kamble R, Sharma A, Kumar M, Saxena AK. Effect of Re on product yields and deactivation patterns of naphtha reforming catalyst. *J Mol Catal A*. 2008;282:74–79.
25. Carvalho LS, Pieck CL, Rangel MC, Figoli NS, Grau JM, Reyes P, Parera JM. Trimetallic naphtha reforming catalysts. I. Properties of the metal function and influence of the order of addition of the metal precursors on Pt–Re–Sn/-Al_2O_3–Cl. *Appl Catal A*. 2004;269:91–103.
26. Hou K, Hughes R. Preparation of thin and highly stable Pd/Ag composite membranes and simulative analysis of transfer resistance for hydrogen separation. *J Membr Sci*. 2003;214:43–55.
27. Cheng YS, Peña MA, Fierro JL, Hui DCW, Yeung KL. Performance of alumina, zeolite, palladium, Pd–Ag alloy membranes for hydrogen separation from Towngas mixture. *J Membr Sci*. 2002;204:329–340.
28. Nam SE, Lee KH. Hydrogen separation by Pd alloy composite membranes: introduction of diffusion barrier. *J Membr Sci*. 2001;192:177–185.
29. Okazaki J, Tanaka DAP, Tanco MAL, Wakui Y, Mizukami F, Suzuki TM. Hydrogen permeability study of the thin Pd–Ag alloy membranes in the temperature range across the α-β phase transition. *J Membr Sci*. 2006;282:370–374.
30. Baker RW. Future directions of membrane gas separation technology. *Ind Eng Chem Res*. 2002;41:1393–1411.
31. Dittmeyer R, Höllein V, Daub K. Membrane reactors for hydrogenation and dehydrogenation processes based on supported palladium. *J Mol Catal A*. 2001;173:135–184.
32. Unemotoa A, Kaimaia A, Satoa K, Otakea T, Yashiroa K, Mizusakia J, Kawadaa T, Tsunekib T, Shirasakib Y, Yasuda I. The effect of co-existing gases from the process of steam reforming reaction on hydrogen permeability of palladium alloy membrane at high temperatures. *Int J Hydrogen Energy*. 2007;32:2881–2887.
33. Streeter VL, Wylie EB, Bedford KW. *Fluid Mechanics*, 9th ed. Boston: WCB McGraw-Hill Inc., 1998.
34. Rase RF. *Chemical Reactor Design for Process Plants*, Vol. 2. New York: Wiley, 1977.
35. Uemiya S. State-of-the-art of supported metal membranes for gas separation. *Sep Purif Methods*. 1999;28:51–85.
36. Rahimpour MR, Esmaili S, Bagheri GNA. Kinetic and deactivation model for industrial catalytic naphtha reforming. *Iran J Sci Technol Trans B Technol*. 2003;27:279–290.
37. Fogler HS. *Elements of Chemical Reaction Engineering*, 2nd ed. Englewood Cliffs, NJ: Prentice-Hall, 1992.
38. Abo-Ghander NS, Grace JR, Elnashaie SSEH, Lim CJ. Modeling of a novel membrane reactor to integrate dehydrogenation of ethylbenzene to styrene with hydrogenation of nitrobenzene to aniline. *Chem Eng Sci*. 2008;63:1817–1826.
39. Balakotaiah V, Luae D. Effect of flow direction on conversion in isothermal radial flow fixed-bed reactors. *AIChE J*;442–450.1981;27:442–450.
40. Hlavkek V, Kubicek M. Modeling of chemical reactors-XXV, cylindrical and spherical reactor with radial flow. *Chem Eng Sci*;177–186. 1972;27:177–186.
41. Shampine LF, Reichelt MW. The Matlab ODE suite. *SIAM J Sci Comput*. 1997;18:1–22.
42. *Operating Data of Catalytic Reformer Unit*, Domestic Refinery. 2005.
43. Perry RH, Green DW, Maloney JO. *Perry's Chemical Engineers' Handbook*, 7th ed. New York: McGraw-Hill, 1997.
44. Smith JM. *Chemical Engineering Kinetics*. New York: McGraw-Hill, 1980.
45. Rice RG, Do D. *Applied Mathematics and Modeling for Chemical Engineers*. New York: Wiley, 1995.
46. Kirkpatrik S, Gelatt CD, Vechhi MP. Optimization by simulated annealing. *Science* 1983;220:671–680.
47. Schwefel HP. *Numerical Optimization of Computer Models*. New York: Wiley, 1981.

48. Goldberg DE. *Genetic Algorithms in Search, Optimization, and Machine Learning*. Reading, MA: Addison-Wesley, 1989.
49. Davis L. *Handbook of Genetic Algorithms*. New York: Van Nostrand Reinhold, 1991.
50. Price K, Storn R. Differential evolution—a simple evolution strategy for fast optimization. *Dr. Dobb's J*. 1997;22:18–24.
51. Babu BV, Angira R. Modified differential evolution (MDE) for optimization of non-linear chemical processes. *Comput Chem Eng*. 2006;30:989–1002.
52. Babu BV, Munawar SA. Differential evolution strategies for optimal design of shell-and-tube heat exchangers. *Chem Eng Sci*. 2007;62:3720–3739.

Appendix A: Auxiliary Correlations

Gas phase viscosity

Viscosity of reactants and products is obtained from the following formula:

Table A1. Constant of Eq. A1 for Reactant and Product

Component	C_1	C_2	C_3	C_4
C_nH_{2n+2}	4.1306×10^{-8}	0.9074	78.2449	0
C_nH_{2n-6}	3.6249×10^{-7}	0.6063	208.5202	0
C_nH_{2n}	3.6744×10^{-7}	0.5868	235.1696	0
H_2	1.797×10^{-7}	0.6850	−0.59	140
L.E = Light ends	4.9054×10^{-8}	0.90125	0	0

Table A2. Constant of Eq. A2 for Reactant and Product

Component	$C_1 \times 10^{-5}$	$C_2 \times 10^{-5}$	$C_3 \times 10^{-3}$	$C_4 \times 10^{-5}$	C_5
C_nH_{2n+2}	1.3781	4.4988	1.6369	3.053	746.85
C_nH_{2n-6}	1.166	4.6381	1.672	3.2894	781.46
C_nH_{2n}	0.8102	3.4545	1.5531	2.459	700.922
H_2	0.27617	0.0956	2.466	0.037	567
L.E = Light ends	0.5192	1.9245	1.6265	1.168	723.6

$$\mu = \frac{C_1 T^{C_2}}{1 + \frac{C_3}{T} + \frac{C_4}{T^2}} \tag{A1}$$

where μ is the viscosity in Pa s and T is the temperature in K. Viscosity is at 1 atm.[43] Constants of Eq. A1 for reactant and product are presented in Table A1.

Gas phase heat capacity

Heat capacity of reactants and products at constant pressure is obtained from the following formula:

$$C_p = C_1 + C_2 \left[\frac{\frac{C_3}{T}}{\sin\ h(\frac{C_3}{T})}\right]^2 + C_4 \left[\frac{\frac{C_5}{T}}{\cos\ h(\frac{C_5}{T})}\right]^2 \tag{A2}$$

where C_p is in J/(kmol K) and T is in K.[43]

Constants of Eq. A2 for reactants and products are presented in Table A2. To complete the simulation, extra correlations should be added to the model. In the case of heterogeneous model, because of transport phenomena, the correlations for estimation of heat and mass transfer between two phases should be considered. It is because of the concentration and heat gradient between bulk of the gas phase and the film of gas on the catalyst surface, which caused by the resistance of the film layer.

Heat-transfer correlation

The heat-transfer coefficient between the gas phase and solid phase is obtained by the following correlation.[44]

$$\frac{h_f}{c_p \rho \mu}\left(\frac{c_p \mu}{K}\right)^{2/3} = \frac{0.458}{\varepsilon_b}\left(\frac{\rho u d_p}{\mu}\right)^{-0.407} \tag{A3}$$

Table A3. Molecular Weights and Critical Volumes of the Components and Other Specifications of Feed at Inlet Conditions

Parameter	Value	Dimension
M_{wm}	21.8	g/mol
ρ_g	12.37	kg/m^3
c_{pg}	88.3	kJ/kmol K
μ	2.87×10^{-2}	cp
k	0.181	W/m K
v_{cp}	0.486	m^3/kmol
v_{cn}	0.460	m^3/kmol
v_{ca}	0.375	m^3/kmol
v_{ch}	0.064	m^3/kmol
$M_{cl,e}$	0.124	m^3/kmol
M_{wn}	113.9	g/mol
M_{wp}	115.9	g/mol
M_{wa}	107.9	g/mol

where in the above equation, u is superficial velocity of gas and the other parameters are those of bulk gas phase, d_p is the equivalent catalyst diameter, K is thermal conductivity of gas, ρ, μ are density and viscosity of gas, respectively, and ε is void fraction of catalyst bed. Molecular weights and critical volumes of the components and other specifications of feed at inlet conditions are reported in Table A3.

Appendix B: Orthogonal Collocation Method

Jacobi polynomials

The Jacobi function, $J_N{}^{(\alpha,\beta)}(x)$, is a polynomial of degree N that is, orthogonal with respect to the weighting function $x^\beta(1-x)^\alpha$. The Jacobi polynomial of degree N has the power series as follow:

$$J_N{}^{(\alpha,\beta)}(x) = \sum_{i=0}^{N} (-1)^{N-i} \gamma_{N,i} x^i \tag{B1}$$

The domain of x is in the range [0, 1].

The evaluation of coefficients is done by using the following recurrence formula

$$\frac{\gamma_{N,i}}{\gamma_{N,i-1}} = \frac{N-i+1}{i} \cdot \frac{N+i+\alpha+\beta}{i+\beta} \tag{B2}$$

Starting with

$$\gamma_{N,0} = 1 \tag{B3}$$

$\gamma_{N,i}$ are constant coefficients, and α and β are parameters characterizing the polynomials.

Lagrange interpolation polynomials

For a given set of data points (x_1,y_1), (x_2,y_2), …, (x_N,y_N), and (x_{N+1}, y_{N+1}) an interpolation formula passing through all $(N + 1)$ points is an Nth degree polynomial. A suitable interpolation polynomial for the orthogonal collocation method is Lagrange interpolation polynomial, which passes through interior collocation points, roots of Jacobi polynomials, and it is expressed as

$$y_N(x) = \sum_{j=1}^{N+1} y_j l_j(x) \tag{B4}$$

where y_N is the Nth degree polynomial, y_i is the value of y at the point x_i, and $l_i(x)$ is defined as

$$l_i(x) = \prod_{\substack{j=1 \\ j\neq i}}^{N+1} \frac{(x - x_j)}{(x_i - x_j)} \tag{B5}$$

Furthermore,

$$l_i(x_j) = \begin{cases} 0 & i \neq j \\ 1 & i = j \end{cases} \tag{B6}$$

The first and second derivative at the interpolation points are:

$$\frac{dy_N(x_i)}{dx} = \sum_{j=1}^{N+1} \frac{dl_j(x_i)}{dx} y_j \tag{B7}$$

$$\frac{d^2y_N(x_i)}{dx^2} = \sum_{j=1}^{N+1} \frac{d^2l_j(x_i)}{dx^2} y_j \tag{B8}$$

for $i = 1,2\ldots,N, N + 1$

The first derivative vector, composed of $(N + 1)$ first derivatives at the $(N + 1)$ interpolation points is:

$$y'_N = \left[\frac{dy_N(x_1)}{dx}, \frac{dy_N(x_2)}{dx}, \ldots, \frac{dy_N(x_N)}{dx}, \frac{dy_N(x_{N+1})}{dx}\right]^{\mathrm{T}} \tag{B9}$$

Similarly, the second derivative vector is defined as

$$y''_N = \left[\frac{d^2y_N(x_1)}{dx^2}, \frac{d^2y_N(x_2)}{dx^2}, \ldots, \frac{d^2y_N(x_N)}{dx^2}, \frac{d^2y_N(x_{N+1})}{dx^2}\right]^{\mathrm{T}} \tag{B10}$$

The function vector is defined as values of y at $(N + 1)$ collocation points as

$$y = [y_1, y_2, y_3, \ldots, y_N, y_{N+1}]^{\mathrm{T}} \tag{B11}$$

By means of these definitions of vectors y and derivative vectors, the first and second derivative vectors can be written in terms of the function vector y using matrix notation

$$\begin{aligned} y' &= A.y \\ y'' &= B.y \end{aligned} \tag{B12}$$

where the matrices A and B are defined as:

$$A = \left\{a_{ij} = \frac{dl_j(x_i)}{dx}; i,j = 1,2,\ldots,N,N+1\right\} \tag{B13}$$

$$B = \left\{b_{ij} = \frac{d^2l_j(x_i)}{dx^2}; i,j = 1,2,\ldots,N,N+1\right\} \tag{B14}$$

The matrices A and B are $(N + 1, N + 1)$ square matrices. Once the $(N + 1)$ interpolation points are chosen, then all the Lagrangian building blocks, $l_i(x_i)$, are completely known, and thus the matrices A and B are also known.[45]

Appendix C: DE Optimization Algorithm

The traditional optimization techniques have limited applications. The main problem of these techniques is the possibility of finding the local optimum instead of global one due to their sensitivity to initial guess. Considering this fact, it is essential to develop more practical optimization techniques based on natural phenomena (evolutionary computation) such as simulated annealing (SA),[46] evolution strategies (ESs),[47] genetic algorithms (GAs),[48,49] and DE.[50]

DE is an efficient and simple optimization technique,[51] which is significantly fast and powerful in numerical optimization and is more likely to find a function's true global optimum.[50] Depending on the type of the optimization problem, different strategies and different values of number of population (NP), DE—step size (F), and crossover probability constant (CR) should be determined. The strategies can vary based on the vector to be perturbed, number of difference vectors considered for perturbation, and finally the type of crossover used. The appropriate value chosen for NP in this research is 100. DE step size lies in the range of 0.5–1.0. The crossover probability constant is in the range of 0.0–1.0. Generally, CR should be as large as possible.[52] More details of basic version of DE, its strategies, and choosing the operating parameters are presented by Babu and Angira[51] and Babu and Munawar.[51]

Manuscript received Aug. 10, 2010, and revision received Nov. 9, 2010.